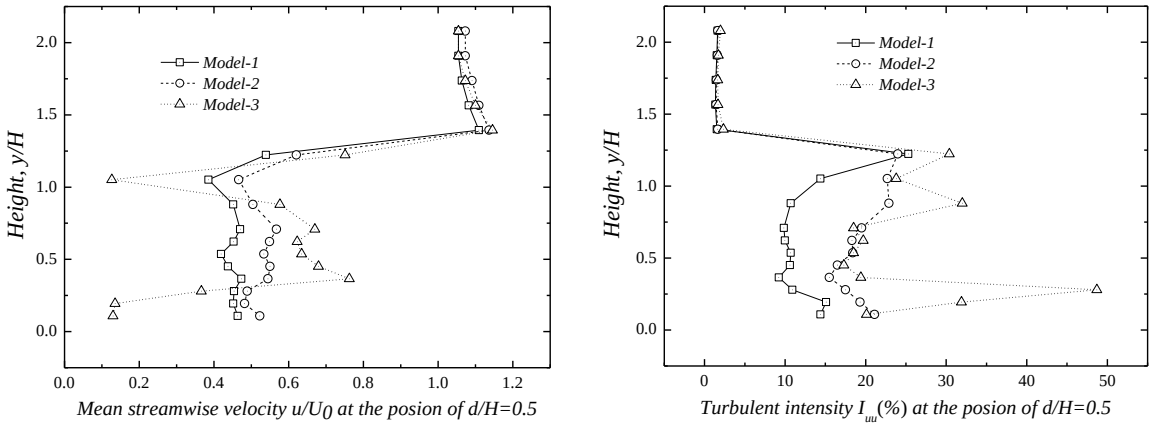

(a) (b)

Fig. 9 Mean streamwise velocity and turbulence intensity profiles of the flow field as a function of height at the position of *d/H=0.5*. (a) mean velocity profiles and (b) turbulence intensity profiles. *H*=height of the wind barrier, U_0= free-stream wind velocity (11m/s), *U(y)*= wind velocity at height *y*, *d*=distance to the barrier

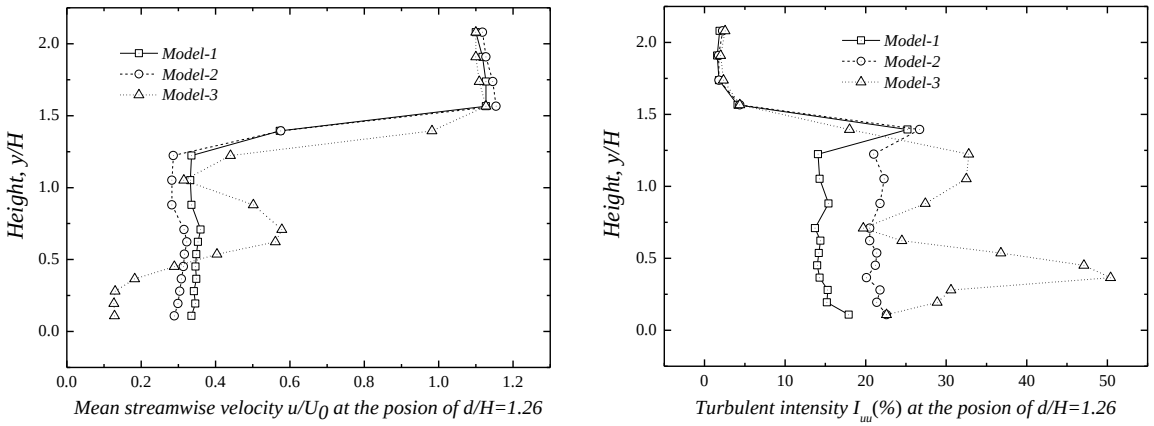

(a) (b)

Fig. 10 Mean streamwise velocity and turbulence intensity profiles of the flow field as a function of height at the position of *d/H=1.26*. (a) mean velocity profiles and (b) turbulence intensity profiles. *H*=height of the wind barrier, U_0= free-stream wind velocity (11m/s), *U(y)*= wind velocity at height *y*, *d*=distance to the barrier

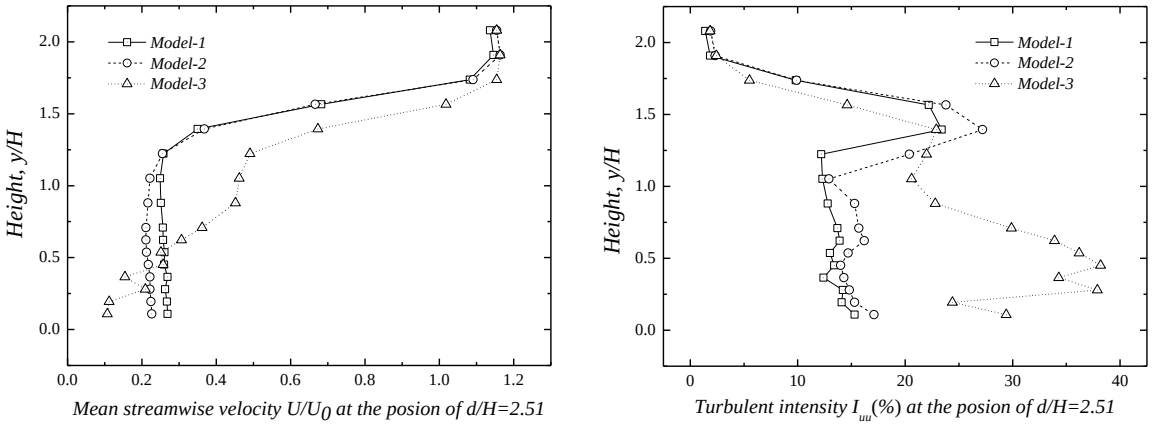

(a) (b)

Fig. 11 Mean streamwise velocity and turbulence intensity profiles of the flow field as a function of height at the position of *d/H=2.51*. (a) mean velocity profiles and (b) turbulence intensity profiles. *H*=height of the wind barrier, U_0= free-stream wind velocity (11m/s), *U(y)*= wind velocity at height *y*, *d*=distance to the barrier

3.1.2 Effects of different forms

Two different forms: porous (Model-2) and bar-type (Model-3) are used to explore the effects of different forms. Fig.7~Fig.11 show the streamwise velocity and turbulence intensity profiles of the flow field as a function of height at different positions. As shown in Fig.7 and Fig.8, the streamwise velocity and turbulence intensity profiles of the flow field are almost similar upwind of the barrier, revealing that the forms of the barrier have little impact on the characteristics of flow field upwind of the barrier. As for the flow field downwind of the barrier (Fig.9~Fig.10), the structure forms of wind barriers have a significant impact on the mean streamwise velocity and turbulence intensity profiles below the height of shear layer. Especially for the distance of 0.5H away from the barrier, great differences of mean streamwise velocity and turbulence intensity profiles under two forms of barriers are found. This is mainly because that some measured points just locate behind the barrier blades and the rest of points just are situated between the adjacent two barrier blades. So the flow fields downwind of the bar-type barrier are relatively uneven compared to the porous barrier. With the increasing of the distances away from the barrier, the difference degrees of mean streamwise velocity profiles decrease, while the differences of turbulence intensity profiles are still great. The flow field passing through porous barriers is likely to be more stable compared to the bar-type barriers. In general, the porous barrier may give a better protection than the bar-type barrier, from the aspect of flow field.

Assessment of the shelter effect of fences should consider not only the absolute reduction in wind velocity, but also the area or distance that is sheltered. So the protected distances of porous barriers and bar-type barriers are further explored. Fig.12 shows the mean streamwise velocity as a function of distance from barriers at the height of *y/H=0.54* (*y=1.88m*) above the surface of wind tunnel. The measuring height (*y=1.88m*) is close to the height of center line of the train body for CRH2 (1.95m above the orbit). Looking at the result, mean streamwise velocities downwind of the barrier are much smaller than free-stream wind velocity. With the changes of the distances away from the barrier (from -1.0H to 2.51H), the mean streamwise velocities for the height of *y/H=0.54* decrease generally. At the distance of 3.0H, the mean streamwise velocity increases obviously at the case of Model-3, while slightly increasing at the case of Model-2. With the increasing of the distance away from the barrier (from 4.0H to 8.0H), the mean streamwise velocities decrease. On the whole, the location of 8H downwind of the barrier is still in the protection zone of barriers at two cases of Model-2 and Model-3.

In order to evaluation the effect of barriers at two cases of Model-2 and Model-3. Turbulence intensity as a function of the relative distance to the wind barrier is also tested (see Fig.13). It is obviously that the turbulence intensity at the case of Model-2 is more uniform compared to the case of Model-3. With the changes of the distances away from the barrier (from -1.0H to 2.51H), the difference of turbulence intensity increases at first and then decreases.

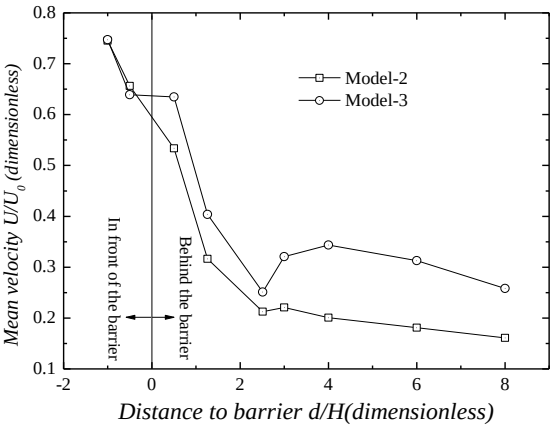

Fig. 12 Mean velocity as a function of the relative distance to the wind barrier for the height of *y/H=0.54* above the bottom of wind tunnel

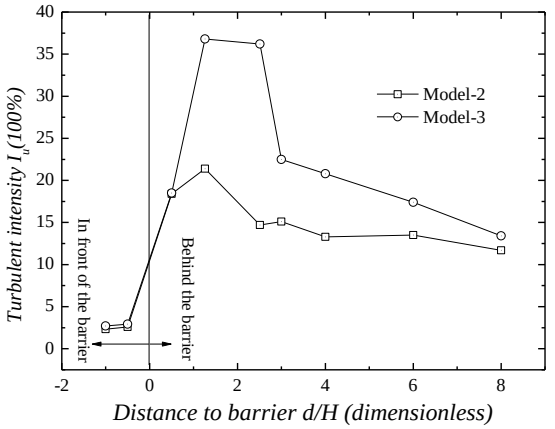

Fig. 13 Turbulence intensity as a function of the relative distance to the wind barrier for the height of *y/H=0.54* above the bottom of the wind tunnel

3.2 Aerodynamic wind loads

The aerodynamic wind loads on barrier blades have to be taken into account in design phase because they cause stress on structures which could lead to safety problems. In the force test, the form 2 is adopted. Form 2 is “long+short+long” which is composed of Blade B、Blade A and Blade C. The Blade A is used for testing (see Fig.14).

A balance (see Fig. 15) is used in the force tests whose range is 5kg and the accuracy is 0.5%. The sampling time and the sampling frequency are set as 120s and 142Hz, respectively. Besides, the sampling frequency is high enough to record the fluctuating signal of the aerodynamic forces acting on the barrier blades. The average of drag forces is used to calculate the aerodynamic coefficients.

The aerodynamics of the wind barrier blades are tested by a balance, and the drag coefficient of the barrier blade is given by

$$C_H = \frac{F_H}{0.5\rho U^2 HL} \tag{1}$$

Where, F_H is the drag force of wind barrier blades. Term H is the height of barrier blades and L is the length of barrier blades. Term U is the velocity of the approach flow and ρ is the air density.

Three kinds of wind velocities (6, 8, 10m/s) are used in the tests. The average of three corresponding results is regarded as the final value. The tested aerodynamic drag coefficients of barrier blades with respect to three cases: Model-1, Model-2 and Model-3 are depicted in Fig. 16. It can be seen that the drag coefficient (C_H) is mainly affected by the location of blades. The aerodynamic drag coefficients of barrier blades close to the wall (A1) and near the column on the right (A11) are relatively small due to the effect of wall and columns on the approach flow, possibly. From left to right (see Fig.14), drag coefficients of barrier blades at three cases increase at first and then decrease. The maximum and minimum of drag coefficients of barrier blades are 0.936 and 0.744 at the case of Model-1, respectively. The maximum and minimum of drag coefficients of barrier blades are 0.911 and 0.708 at the case of Model-2, respectively. The maximum and minimum of drag coefficients of barrier blades are 1.617 and 0.967 at the case of Model-3, respectively.

Differences of drag coefficients between Model-1 and Model-2 (The porosities of barrier blades being all 36.5%) are attributed to two aspects: fluctuating force and pore size. When free-

stream wind field passing through barriers, airflow changes to be unstable. It leads to the existing of fluctuating force, which will make a contribution to the drag force of blades and the fluctuating force is related to the pore size of the barrier blade. As for the case of Model-3, the porosities of barrier blades are 0%. So the drag coefficients of barrier blades at the case of Model-3 are larger than drag coefficients of barrier blades at the cases of Model-1 and Model-2, generally.

Firstly, the distribution law of drag coefficients of barrier blades located at different positions is investigated. Then we want to get the drag coefficients of the whole barrier. The drag coefficients of the whole barrier can be calculated by the following equations:

$$F_H = 0.5\rho U^2 C_H HL \tag{2}$$

$$\sum_{i=1} F_{Hi} = F_{HZ} \tag{3}$$

$$C_{HZ} = \frac{\sum_{i=1} C_{Hi} \times H_i}{H_Z} \tag{4}$$

Where, F_{Hi}、C_{Hi} are the drag forces and drag coefficients of wind barrier blades, respectively. F_{HZ}、C_{HZ} are the drag forces and drag coefficients of whole wind barriers, respectively. H_i (see Table 1)、H_Z (3.5m) are the heights of wind barrier blades and whole wind barriers, respectively.

The tested aerodynamic drag coefficients of whole barriers with respect to three cases: Model-1, Model-2 and Model-3 are depicted in Table2. It can be seen that the drag coefficients of porous barriers (Model-1 and Model-2) are about the same. Some differences exist between the bar-type barrier (Model-3) and porous barriers (Model-1 and Model-2). Drag coefficient of the whole barrier at case of Model-3 is the relative minimum (0.675).

Fig. 14 Distribution diagram of wind barrier blades

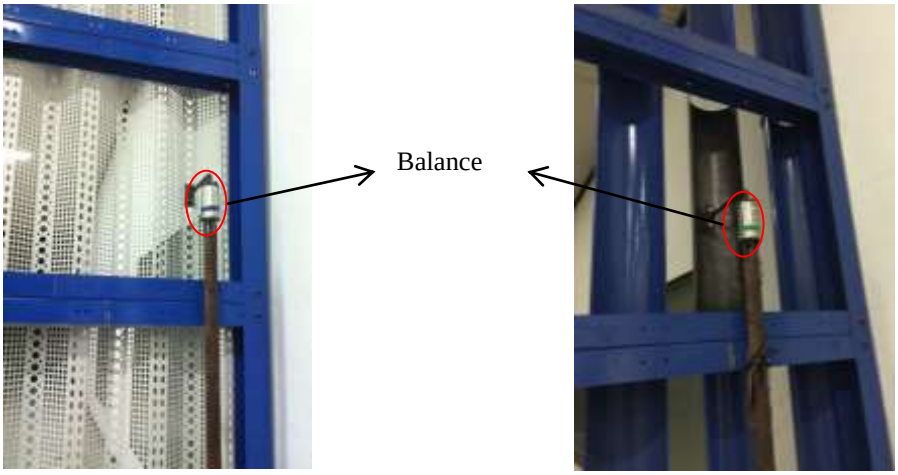

(a) Porous barrier blades (b) Bar-type barrier blades

Fig. 15 Tests of aerodynamic force for wind barriers

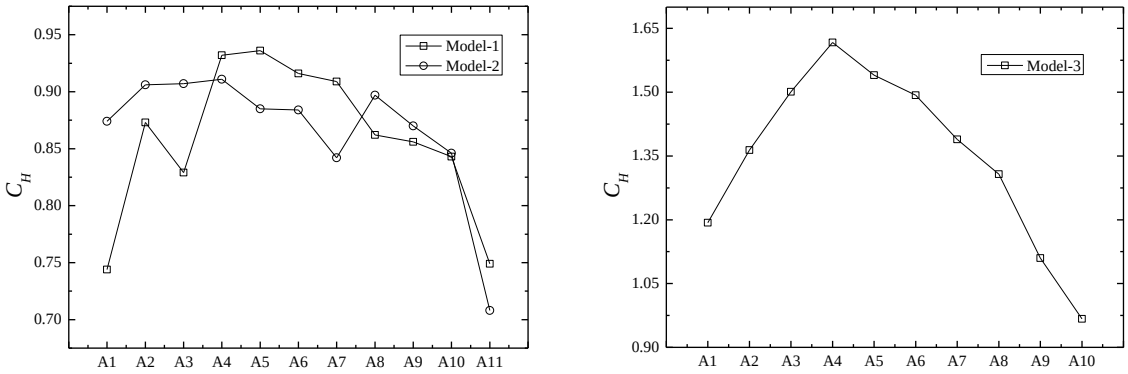

Fig. 16 Aerodynamic coefficients of barrier blades at different cases

Table2 Aerodynamic coefficients of the whole barriers at different cases

Case	Model-1	Model-2	Model-3
C_{HZ}	0.777	0.793	0.675

4. Conclusions

In the wind tunnel tests, the characteristics of flow field and aerodynamic loads of wind barrier blades were collected with respect to three cases: Model-1, Model-2 and Model-3, and then the results were analyzed and discussed. At present, the impact of scale effect has not been fully explored. So our results are more believable. The main conclusions are summarized as follows.

1) The location of barrier blades has significant impacts on the aerodynamic drag coefficients of barrier blades. Based on the experimental results, aerodynamic drag coefficients of the blades close to the wall and near the column on the right are relatively small. From left to right, drag coefficients of barrier blades at three cases increase at first and then decrease. The drag coefficients of whole barriers at three cases of Model-1, Model-2 and Model-3 are 0.777, 0.793 and 0.675, respectively.

2) Differences are great for the mean streamwise velocity profiles upwind and downwind of the barrier. There exists an obvious shear layer in the mean streamwise velocity profile downwind of the barrier. Upwind of the barrier, mean streamwise velocities increase with the

increasing of the height above the surface. At the distance of -0.5H and -1.0H away from the barrier, an intersection point is found on the profiles. Moreover, the height of intersection point is close to the height of shear layer of mean streamwise velocity profiles downwind of the barrier.

3) As for the porous barriers (Model-1 and Model-2), the pore size of the barrier blade has a slight influence on mean streamwise velocities and turbulence intensity upwind of the barrier. However, an obvious influence on mean streamwise velocities and turbulence intensity is found at the distance of 0.5H away from the barrier. At the distances of 1.26H and 2.51H, the influence on mean streamwise velocities is less obvious, while it has some influence on the turbulence intensity.

4) Slight influence of different forms of barriers (porous and bar-type) on the mean streamwise velocities and turbulence intensity is found upwind of the barrier, while great influence exists downwind of the barrier. On the whole, the mean streamwise velocities and turbulence intensity downwind of the porous barrier are more uniform than the bar-type barrier's. Moreover, values of mean streamwise velocities and turbulence intensity of the porous barrier at the same position are relatively smaller.

5) From distance of -0.5H to distance of 8H away from the barrier, mean streamwise velocities decrease generally. The turbulence intensity increases at first and then decreases. Our observations reveal that the distance of 8H downwind of the barrier is still in the effective protection area of barriers.

Acknowledgments
The research described in this paper was supported by the National Natural Science Foundation of China (Grant No. NNSF-U1334201), the National Basic Research Program of China ("973" Project) (Grant No. 2013CB036206), and the Sichuan Province Youth Science and Technology Innovation Team (Grant No. 2015TD0004).

References:

Richardsona, G. (1995), "Full-scale measurements of the effect of a porous windbreak on wind spectra", *J WIND ENG IND AEROD*., **54-55** 611-619.

Wang, D., Wang, B. and Chen, A. (2013), "Vehicle-induced aerodynamic loads on highway sound barriers part1: field experiment", *WIND STRUCT*., **17**(4), 435-449.

Dierickx, W., Gabriels, D. and Cornelis, W. (2001), "A wind tunnel study on wind speed reduction of technical textiles used as windscreen", *GEOTEXT GEOMEMBRANES*., **19**(1), 59-73.

Dierickx, W., Cornelis, W.M. and Gabriels, D. (2003), "Wind Tunnel Study on Rough and Smooth Surface Turbulent Approach Flow and on Inclined Windscreens", *BIOSYST ENG*., **86**(2), 151-166.

Dong, Z., Luo, W., Qian, G. and Wang, H. (2007), "A wind tunnel simulation of the mean velocity fields behind upright porous fences", *AGR FOREST METEOROL*., **146**(1), 82-93.

Wu, X., Zou, X., Zhang, C., Wang, R., Zhao, J. and Zhang, J. (2013), "The effect of wind barriers on airflow in a wind tunnel", *J ARID ENVIRON*., **97** 73-83.

Santiago, J.L., Martín, F., Cuerva, A., Bezdenejnykh, N. and Sanz-Andrés, A. (2007), "Experimental and numerical study of wind flow behind windbreaks", *ATMOS ENVIRON*., **41**(30), 6406-6420.

Bitog, J.P., Lee, I.B., Shin, M.H., Hong, S.W., Hwang, H.S., Seo, I.H., Yoo, J.I., Kwon, K.S., Kim, Y.H. and Han, J.W. (2009), "Numerical simulation of an array of fences in Saemangeum reclaimed land", *ATMOS ENVIRON*., **43**(30), 4612-4621.

Telenta, M., Batista, M., Biancolini, M.E., Prebil, I. and Duhovnik, J. (2015), "Parametric numerical study of wind barrier shelter", *WIND STRUCT*., **20**(1), 75-93.

Huoyue, X., Yongle, L. and Bin, W. (2015), "Aerodynamic interaction between static vehicles and wind barriers on railway bridges exposed to crosswinds", *WIND STRUCT*., **20**(2), 237-247.

Suzuki, M., Tanemoto, K. and Maeda, T. (2003), "Aerodynamic characteristics of train/vehicles under cross winds", *J WIND ENG IND AEROD*., **91**(1–2), 209-218.